Cell Reports
Physical Science

CellPress
OPEN ACCESS

Article

An integrated solar-driven system produces electricity with fresh water and crops in arid regions

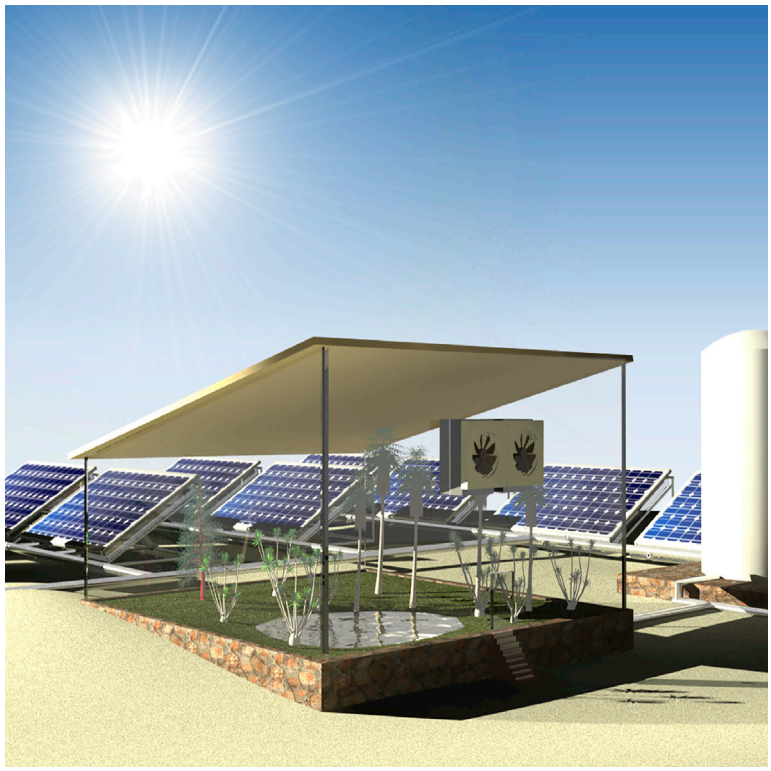

The centralized production of electricity, water, and food coupled with long-distance transmission and transportation is neither possible nor cost effective for off-grid communities. Wang et al. report a water-electricity-crop co-production system based on atmospheric water harvesting, which is promising to make a solid contribution to the global water-energy-food nexus.

Renyuan Li, Mengchun Wu, Sara Aleid, Chenlin Zhang, Wenbin Wang, Peng Wang

peng.wang@kaust.edu.sa

Highlights

Recycle waste heat from PV panels to produce fresh water from the atmosphere

Cool down PV panel and increase its electricity generation performance

Integrated system (WEC^{2}P) produces electricity with fresh water and crops

Application is with minimal geological constrain

Li et al., Cell Reports Physical Science 3, 100781
March 16, 2022
https://doi.org/10.1016/j.xcrp.2022.100781

Please cite this article in press as: Li et al., An integrated solar-driven system produces electricity with fresh water and crops in arid regions, Cell Reports Physical Science (2022), https://doi.org/10.1016/j.xcrp.2022.100781

Cell Reports
Physical Science

Article

An integrated solar-driven system produces electricity with fresh water and crops in arid regions

Renyuan Li,[1] Mengchun Wu,[1] Sara Aleid,[1] Chenlin Zhang,[1] Wenbin Wang,[1] and Peng Wang[1,2,3,*]

SUMMARY

Stable supplies of water, energy, and food are the most essential factors to universal achievements of the United Nation's Sustainable Developments Goals (SDGs) by 2030. This work reports a self-sustained and solar-driven, integrated water-electricity-crop co-production system (WEC^{2}P). The design of WEC^{2}P is based on the atmospheric water adsorption-desorption cycle (1) to generate cooling power for photovoltaic (PV) cells to increase their electricity generation performance or (2) to sustainably produce fresh water from atmospheric water vapor to support crop growth. During the 3-month-long outdoor field test, the WEC^{2}P successfully reduced the temperature of PV panels by up to 17°C and increased their electricity generation by up to 9.9% in the PV cooling mode. Meanwhile, it produced water to irrigate crops (i.e., water spinach) hosted in an integrated plant-growing unit in Saudi Arabia, with a crop surviving rate of 95%. Thereby, WEC^{2}P may represent a meaningful contribution to the global water-energy-food nexus.

INTRODUCTION

Stable supply of water, energy, and food are the three of the most essential and indispensable factors of modern life and are keys to universal achievements of the United Nation's Sustainable Developments Goals (SDGs) by 2030.[1–4] However, the already over-stressed water-energy-food nexus is further complicated by the ongoing climate change,[5–9] which urgently calls for holistic approaches to address the conflicts regarding allocation of resources among these sectors and, in doing so, in a minimal-carbon manner.

Globally speaking, there are an estimated ~2 billion people lacking safe drinking water,[10,11] 800 million people without access to electricity,[12] and ~700 million people living in constant famine.[13] Achieving the SDGs by 2030 will largely depend on how to enhance the livelihoods of the "bottom billion,"[14] most of whom live in rural areas and 300 million of whom live in Africa, South-Asia, and the Middle East with arid or semi-arid climates.[10,12,13] Clearly, centralized generation of both electricity and drinking water coupled with long-distance transmission and transportation in these regions is neither possible nor cost-effective due to the lack of financial resources and also to low population density.[15–17] At the same time, low-barrier-of-entry decentralized approaches are nowadays believed most suited to economically provide electricity and water on site for point of consumption (POC) in these rural regions.[18–20]

The atmosphere constantly preserves more than 12,900 billion tons of pre-distilled fresh water, and atmospheric water is continuously replenished by global water

[1]Water Desalination and Reuse Center, Division of Biological and Environmental Science and Engineering, King Abdullah University of Science and Technology, Thuwal 23955-6900, Saudi Arabia

[2]Department of Civil and Environmental Engineering, the Hong Kong Polytechnic University, Hung Hom, Hong Kong, China

[3]Lead contact

*Correspondence: peng.wang@kaust.edu.sa

https://doi.org/10.1016/j.xcrp.2022.100781

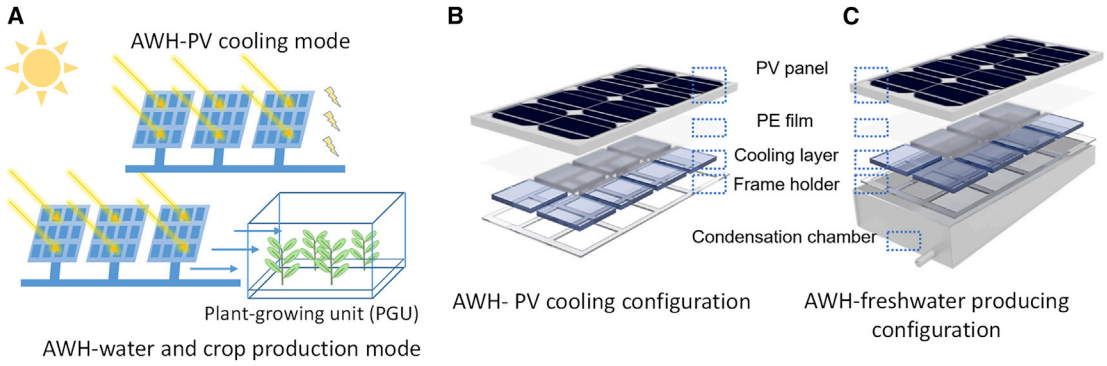

Figure 1. Schematic of the system configuration

(A–C) (A) Working principles of WEC^{2}P. (B and C) Device configurations of (B) AWH-PV cooling and (C) AWH water production are shown.

circulation.[21,22] A recent study pointed out that the solar-driven atmospheric-water-harvesting process can potentially fulfill the drinking water demands of 5 L per day per capita for more than two billion people across the globe.[23] Tan's group also reported the use of ambient humidity in the fields of energy harvesting,[24,25] autonomous urban agricultures,[26] and autonomous humidity-management systems.[27] Thereby, the use of atmospheric water as an alternative water resource could be a promising approach to addressing water and energy shortage in off-grid communities and arid or semi-arid regions.

Simultaneously, photovoltaic (PV) panels convert solar energy to produce electricity.[28] PV uses abundant and clean solar energy, requires low and flexible capital investment, and is suitable at any scale, all of which makes it an important approach for point-of-application (POA) electricity generation.[29,30] One of our previous studies has utilized the waste heat of a PV panel to drive multistage membrane distillation to produce fresh water from seawater as well as to reduce the temperature of a PV panel, leading to increased electricity generation by the same panel.[31] Another work that involved PV technology in the agricultural sector was reported by Al-Ibrahim et al.,[32] which successfully demonstrated the feasibility of using solar energy to power up the electronic components in a plant-scale greenhouse system in arid regions. Very recently, our work has proposed and proven a PV panel cooling strategy based on atmospheric water vapor adsorption and desorption cycle.[33]

This work proposes a conceptual design and provides a demonstration of an integrated water-electricity-crop co-production system (WEC^{2}P), which is fully solar energy driven, low cost, and suitable for supporting a decentralized lifestyle. A WEC^{2}P system employs atmospheric-water-harvesting (AWH) material (i.e., the sorbent) to capture water vapor from air, typically at night or in the evening; utilizes the heat from a PV panel during the day to drive evaporation of the captured atmospheric water out of the sorbent to cool the panel; collects the evaporated water vapor to generate fresh water; and waters crops fully by the generated fresh water (Figure 1A). The design of WEC^{2}P is so that it offers two easily switchable modes: PV cooling and water-crop production, allowing for high flexibility in practical applications. A theoretical model is developed to guide the system design, three sets of 30 × 60 cm^2 integrated PV panels are fabricated, and the performance of the devices are evaluated by 3-month-long outdoor field tests using these panels as a successful proof of concept. In PV-cooling mode, the PV panels are cooled by up to 17°C and, in turn, increase their electricity generation by up to 9.9% under the field conditions. In water-crop co-production mode tests, the water produced by the panel sets is

able to fully water the model crop: 60 water spinaches, leading to an average stem growth of ~18 cm and a survival rate of 95% after the outdoor growth in Thuwal, Saudi Arabia during summer 2021. The water production and crop growth do not consume any electricity generated by the PV panels. WEC^{2}P has the potential to facilitate the achievement of the SDGs as it provides a promising solution to decentralized water, electricity, and crop production suitable for arid- and semi-arid regions and beyond. It thus represents a meaningful contribution to the global water-energy-food nexus.

RESULTS

Design and assembly of WEC^{2}P

The WEC^{2}P is designed to have two operation modes: AWH-PV cooling mode (Figure 1B) and AWH-water and crop production mode (Figure 1C). The incident sunlight is absorbed and partially converted into electricity by the PV cells, with the rest, typically more than 80% of the adsorbed sunlight, being converted into heat, leading to an enhanced temperature of the PV panel.[33–35] The AWH-cooling layer consists of a polyethylene (PE) anti-corrosion film (~0.04 mm in thickness) and an array of atmospheric water-vapor sorbents, i.e., polyacrylamide-calcium chloride (PAM-$CaCl_2$) hydrogel, as reported in our previous work.[36,37] The PV heat drives the water to evaporate from the sorbent during the daytime, effectively reducing the PV temperature.

To collect the evaporated water vapor during the daytime, a condensation chamber was used as the passive condenser (Figure 1C). In this work, the surface area of the fabricated condensation chamber was 1.6 times that of the overlying PV panel (Note S1). The produced water in the AWH-water production configuration was used to irrigate crops planted inside a plant-growing unit (PGU). The PGU used in this work was designed to passively maintain the internal humidity and temperature within a reasonable range without consuming electricity under normal conditions. By design, the WEC^{2}P system can produce electricity, clean water, and crops with a low carbon footprint.

Model simulation and cooling effect prediction

Theoretically, the cooling performance of the WEC^{2}P system is dominated by three factors: solar irradiance; ambient temperature; and ambient wind speed. A COMSOL model (Note S2; Figure S1) was established to understand the relative contributions from each factor under different ambient conditions, which are essential to guide the design and deployment of the devices under real circumstances. More specifically, three solar irradiances (i.e., 0.8, 1.0, and 1.2 kW/m^2), two ambient temperatures (i.e., 20°C and 40°C), and two wind speeds (i.e., 0.1 and 1.0 m/s) were investigated (Figures S2 and S3).

The simulation results indicate that (1) the wind speed plays the most important role in dissipating heat from the device to the ambient, which can be ascribed to its strong convective heat transfer effect. (2) The ambient temperature plays a critical role that determines the minimum temperature of the WEC^{2}P during both the AWH-PV cooling mode and AWH-water and crop production mode. (3) Solar irradiance can largely influence the temperature of PV in AWH-water and crop production mode, especially when the ambient temperature is high and wind speed is low (i.e., 0.1 m/s in this case). (4) The installation of a heat fin can effectively reduce the PV temperature, especially under strong sunlight irradiation and hot and quiescent weather conditions, due to its enlarged heat exchange area. However, the condensation chamber without the use of heat fin is also able to produce fresh water

effectively. The simulation results imply the feasibility of WEC^{2}P in effectively cooling down PV panels and producing water from air without increasing the PV-panel temperature.

AWH-PV cooling test and electricity generation evaluation

Two PV panels with the pre-evaluated average electricity conversion efficiency of 15.0% and 15.1% were used for AWH cooling tests (Notes S3 and S4; Figures S4–S6; Table S1), denoted as "AWH cooling one" and "AWH cooling two" in this section. The AWH cooling performance and the electricity generation increments of PV panels were evaluated in the outdoor conditions (Figures S7–S9) from April 1 to May 10, 2021 for 40 days continuously except the system maintenance dates.

Figure 2A displays the digital photo of the assembled AWH-PV module, showing a close contact between the AWH cooling layer and the backside of the PV panel. The infrared (IR) image during the operation demonstrated a significant PV temperature drop due to the AWH cooling. Furthermore, no apparently hot or cold local spots were observed in the cooling layer, indicating the hydrogels were evenly attached with the PV panel (Figures 2B, 2C, 2E, and 2F). As expected, the peak power of the PV panels in the AWH cooling one and AWH cooling two batches were consistently higher than that of the "without cooling" batch (Figures S11A, S11C, and S11D). The temperature profiles of all PV panels during the outdoor field tests were acquired with thermocouples that were embedded beneath the solar cell and between the ethyl vinyl acetate (EVA) encapsulant layer and the back sheet. The peak PV operation temperature of the batch without cooling was 70.0°C–81.5°C in April and 64.1°C–73.9°C in May, while the AWH cooling one and AWH cooling two batches showed decreased temperatures by up to 17°C, with an average temperature reduction by 13°C to 14°C (Figures S11B, S11D, and S11F).

Figure 2G surmised the accumulated electricity generation on a daily basis. It should be noted that the collection of data during the field tests was interrupted due to system maintenance (e.g., replacement of the lead-acid battery connected with the maximum power point tracker (MPPT) system and upgrade of battery container). During the 40-day AWH-PV cooling test, the total electricity generated by AWH cooling 1, AWH cooling 2, and without cooling was 4,184.0 Wh (581.1 Wh/day/m^2), 4,220.1 Wh (586.1 Wh/day/m^2), and 3,838.2 Wh (533.1 Wh/day/m^2), respectively. The electricity generation increment for AWH cooling one and AWH cooling two were 9.0% and 9.9% relative to the PV panel without cooling.

AWH cooling and fresh water producing test

The same AWH-PV module (AWH cooling 1) was switched to AWH-water production mode (Figures 3A and 3B), which is denoted as "AWH water production" in this section. Please note that no crop production was tested in this part. The condensation chamber was made of an aluminum alloy with a copper nozzle at the lower sidewall. A cotton wick was used, passing through the nozzle to help the extraction of the condensed water into the water-collection bottle (Figure 3B, inset photo). To avoid loss of water from evaporation, the wick was placed inside a silicon tube that bridged the condensation chamber and the collection bottle. Water vapor released from sorbents was condensed inside the condensation chamber and collected in the glass bottle (Figures 3C and 3D).

The working principles of the AWH water collection process were based on alternatively opening and closing the condensation chamber for atmospheric water absorption and clean water condensation process. The outdoor test was performed from

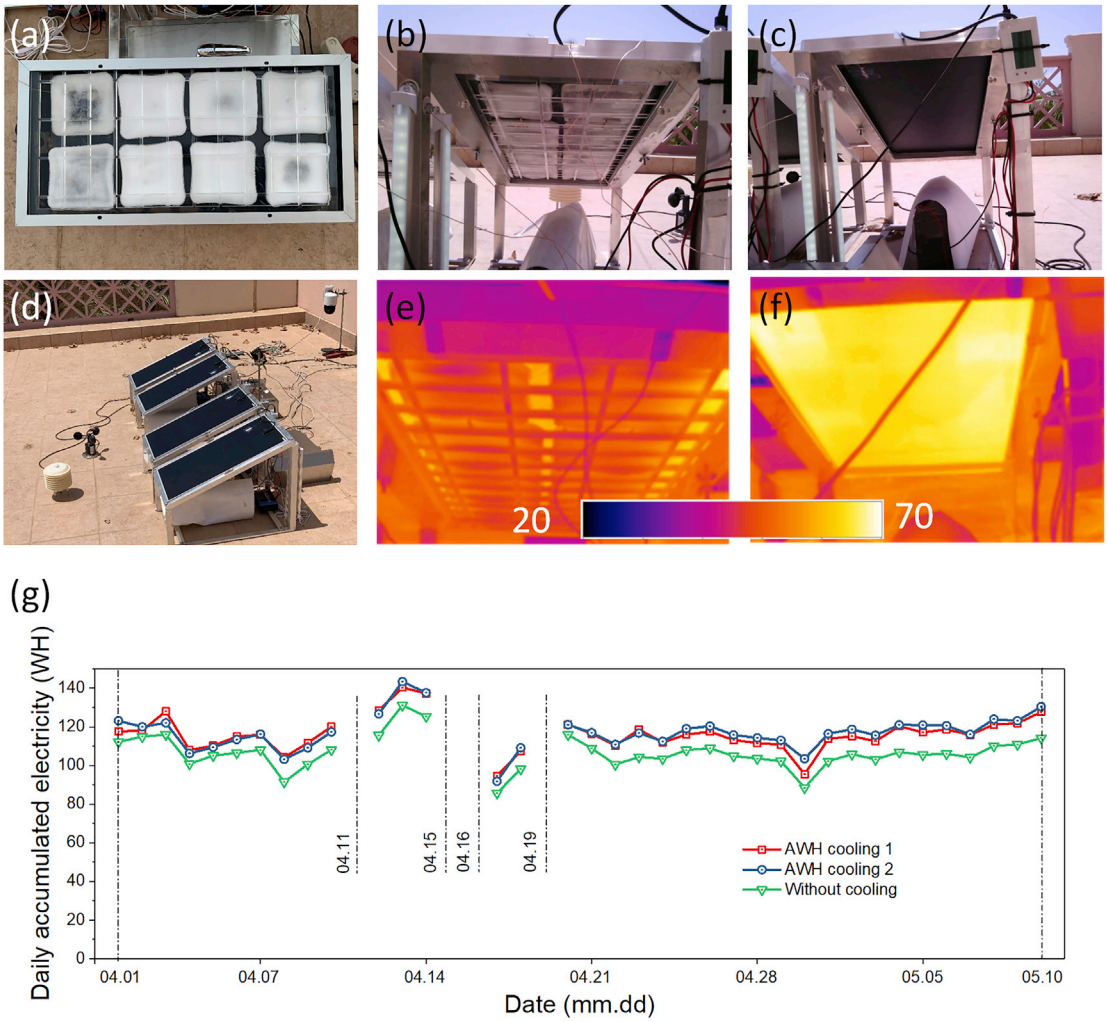

Figure 2. Evaluation of cooling performance and electricity generation increment driven by the AWH cooling process

(A) Digital photo of the backside of the assembled AWH-PV module.

(B and C) Digital photos of the backside of PV panels with and without the AWH cooling layer, respectively.

(D) Digital photo of the field test experimental setup.

(E and F) IR images of PV panels with and without the AWH cooling layer, respectively.

(G) Daily accumulated electricity generation. Note: the missing data points were due to system maintenance on the referred-to dates (April 11, 15, 16, and 19, 2021).

May 12 to June 11, 2021, for 30 days. Details of the experiments can be found in the experimental procedures section. The water collected from the on-site air using the AWH system was transferred from the collection bottle to the reservoir bottle on a daily basis. The on-site peak solar irradiance during the test was ~800 W/m^2 in May and slightly reduced to ~700 W/m^2 in early June (Figures S12A and S13A). The weakened solar irradiance in June could be attributed to several different factors, such as thick clouds and dusty weather. The ambient peak temperature was mostly higher than 40°C during the test (Figures S12B and S13B). The reduced solar irradiance resulted in a compromised electricity generation performance. The peak power of PV in May was mostly ~17.5 W (97.2 W/m^2), while only ~15.6 W (86.7 W/m^2) could be achieved in June. The temperature of the PV panel in the AWH water production batch significantly increased by at least 10°C compared with the one without a condensation chamber. This temperature, however, was still slightly lower

Please cite this article in press as: Li et al., An integrated solar-driven system produces electricity with fresh water and crops in arid regions, Cell Reports Physical Science (2022), https://doi.org/10.1016/j.xcrp.2022.100781

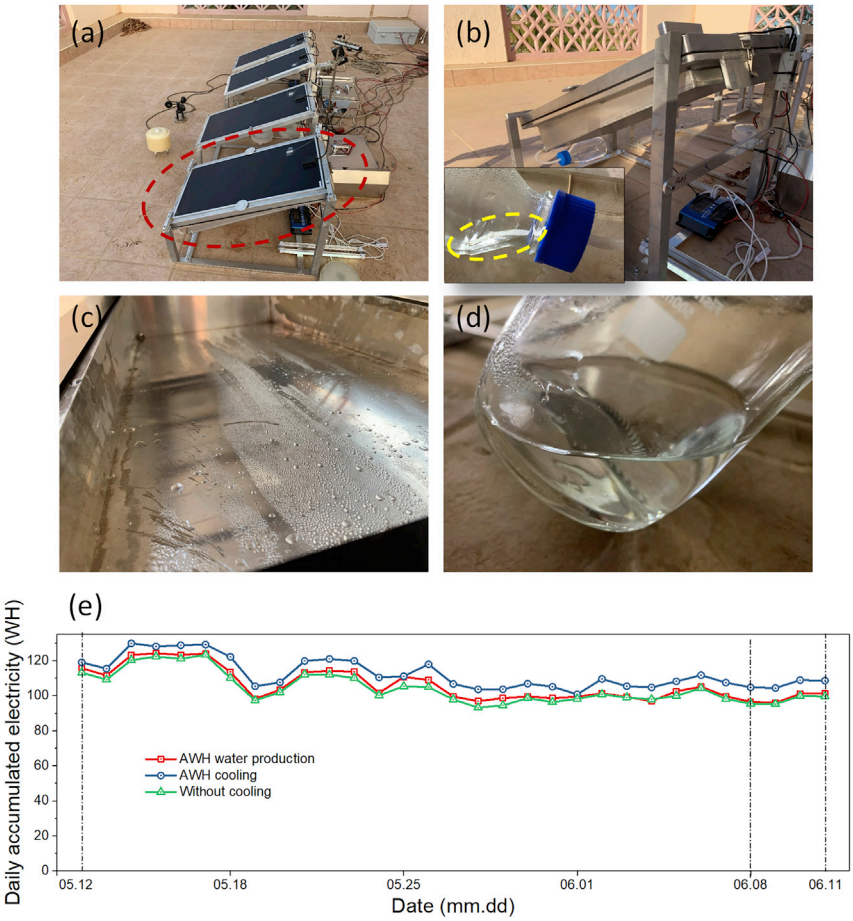

Figure 3. Experimental configuration of AWH-water producing test

(A) Digital photo of the AWH water-producing module (in the red dash circle).

(B) Digital photo of the AWH water-producing module in a closer view. Inset: the water collection bottle was connected with the silicon tube and cotton wick (in the yellow dash circle).

(C) The condensed water droplets inside the condensation chamber.

(D) The collected water within 1 day (picture was taken on May 15, 2021) within a 500 mL glass bottle.

(E) Daily accumulated electricity generation record.

(~1°C–3°C) than that of the PV panel in the without cooling batch due to the sufficient surface area of the condensation chamber, which facilitates heat dissipation. The temperature difference led to the corresponding power differences among the three batches (Figure S14). Moreover, the overall daily accumulated electricity generation in June (Figure 3E) was lower than that in May and April presumably due to the weakened solar irradiance. During the 30-day AWH water producing test, the accumulated electricity generation by AWH water production, AWH cooling, and without cooling batches was 3,292.3 Wh (609.7 Wh/m^2/day), 3,487.8 Wh (645.7 Wh/m^2/day), and 3,232.5 Wh (598.6 Wh/m^2/day), respectively. The electricity generation increment for AWH water producing and AWH cooling was 1.8% and 7.9% compared with the PV panel without cooling.

The experimental results were further compared with the modeling results. The temperature of PV panels observed in the field test was similar to the temperature obtained from COMSOL simulation under similar working conditions. Compared with the ambient conditions on the referred to dates, it can be seen that the daily

water production rate highly depends on the relative humidity (RH) during the night for the atmospheric water vapor sorption process. On the other hand, the solar irradiance along with the ambient temperature during the daytime play a significant role in the clean water condensation process. The volume of water collected during the 30-day test by the device with a PV panel dimension of 0.6 × 0.3 m^2 was 3.4 L. The quality of the produced water was analyzed by total organic carbon-total nitrogen (TOC-TN) analyzer and inductively coupled plasma optical emission spectroscopy (ICP-OES). The ion content and TOC-TN concentration of the produced water fulfilled the World Health Organization (WHO) drinking water standard (Figure S16) regarding these parameters.[38]

Crop production feasibility test of WEC^{2}P in field conditions

The WEC^{2}P field test was performed on June 15–30, 2021 using a modified bench-scale commercialized PGU (modification details can be found in the experimental procedures section). An electronic cooling unit powered by the AWH water-producing module was installed as a preventive measure that was activated only when the temperature inside the PGU exceeded 50°C to avoid overheating of the plants. It should be mentioned that the electronic cooling unit served as a prevention measurement and actually was not operated, as the internal PGU temperature remains below 50°C throughout the test (Figures 4A–4C).

The green-leaf plant, water spinach (*Ipomoea aquatica*), was used as a model crop for the WEC^{2}P field test. In the first step, 60 water spinach seeds were imbibed in 20 mL of the as-collected water from the "AWH cooling and fresh water producing test" for 12 h. A 30-hole stencil plate with a hole diameter of 30 mm was placed on the top of the soil bath to reduce evaporation of water from the soil and separate the growing space of the plants. Then, the soil bath was irrigated with 800 mL of the as-collected water from the reservoir bottles, and the water spinach seeds were subsequently sowed in the soil bath with a planting density of two seeds per hole. In the long-term practical applications, PGU can take advantage of sand and soil from the local sites and nutrients can be supplied from condensed liquid fertilizer during daily irrigation to address the shortage of potting soil in the off-grid and remote arid regions. A control experiment was conducted with a nine-hole stencil and without the PGU and atmospheric water irrigation, other test conditions and parameters being the same (Figure S17).

The PGU was opened during the night from 7:00 p.m. to 7:00 a.m. the next day with a sunlight-shielding net and the perforated board removed for plant breathing. During the daytime, from around 7:00 a.m. to 7:00 p.m. the same day, the PGU remained closed to avoid excessive water loss and sunburn of plants. The soil bath was replenished with ~150 mL of water every evening either solely from the collected water during the daytime or from the collected water and the reservoir bottle when the water productivity was insufficient due to the unsatisfied weather condition. The internal temperature and RH of the PGU were recorded with a Logtag (Figure S18). The RH during the daytime ranged between 69.1% and 89.2%, similar to the ambient RH during the night when the PGU was opened (Figure S19).

A picture of the plant was taken at the same time every morning at around 7:00 a.m. from June 16 to July 1, 2021 to record the plant growing status (Figure 4D). The survival rate was counted based on the surviving plants at the end of the test and the original sowed seeds, which was determined to be 95% (i.e., 57 survived plants versus 60 sowed seeds). On the contrary, no germinated seeds were found in the

Please cite this article in press as: Li et al., An integrated solar-driven system produces electricity with fresh water and crops in arid regions, Cell Reports Physical Science (2022), https://doi.org/10.1016/j.xcrp.2022.100781

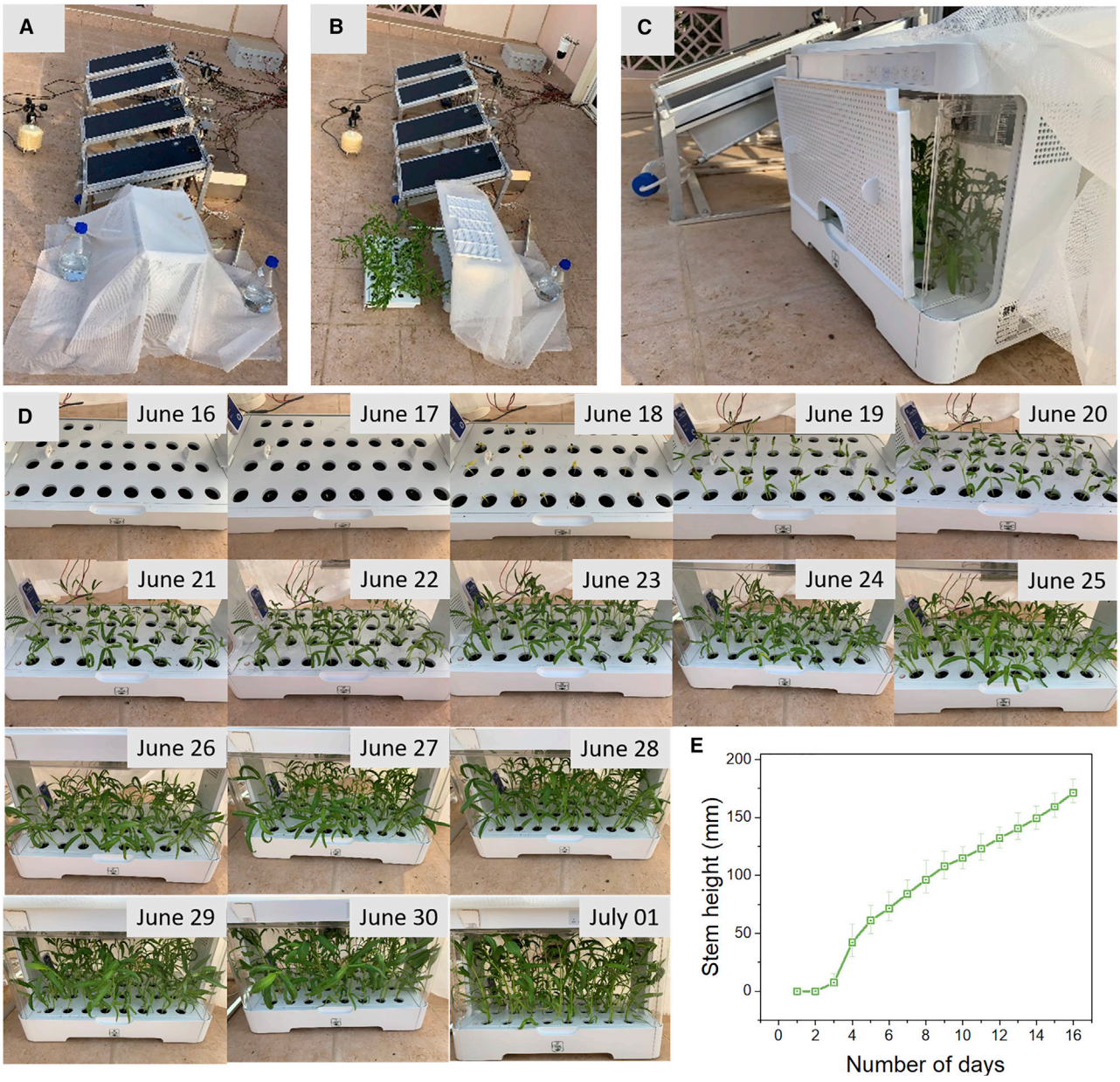

Figure 4. Experimental setup of the integrated water-electricity-crop co-production system (WEC^{2}P)

(A) The digital photo of the deployed PGU. The two 2-L-capacity glass bottles with blue caps were the reservoir bottles that were filled with ~3.4 L of clean water in total from "AWH cooling and fresh water producing test" section.

(B) PGU with soil bath and planted water spinach.

(C) The perforated board sidewall.

(D) Growing status of water spinach.

(E) Stem height of water spinach during the test. The error bars describe the ranges of measured stem heights in the referred-to days.

control experiment throughout the test, and thus, the survival rate of the control experiment was 0%. The stem height of the water spinach was recorded every morning to reflect the growing rate. As seen in Figure 4E, despite the germination stage at the first 5 days, an approximately linear growing rate of the water spinach was observed, which further demonstrated the stability and feasibility of WEC^{2}P. Due to the space constrain of the bench-scale PGU, the test had to be stopped on day

Please cite this article in press as: Li et al., An integrated solar-driven system produces electricity with fresh water and crops in arid regions, Cell Reports Physical Science (2022), https://doi.org/10.1016/j.xcrp.2022.100781

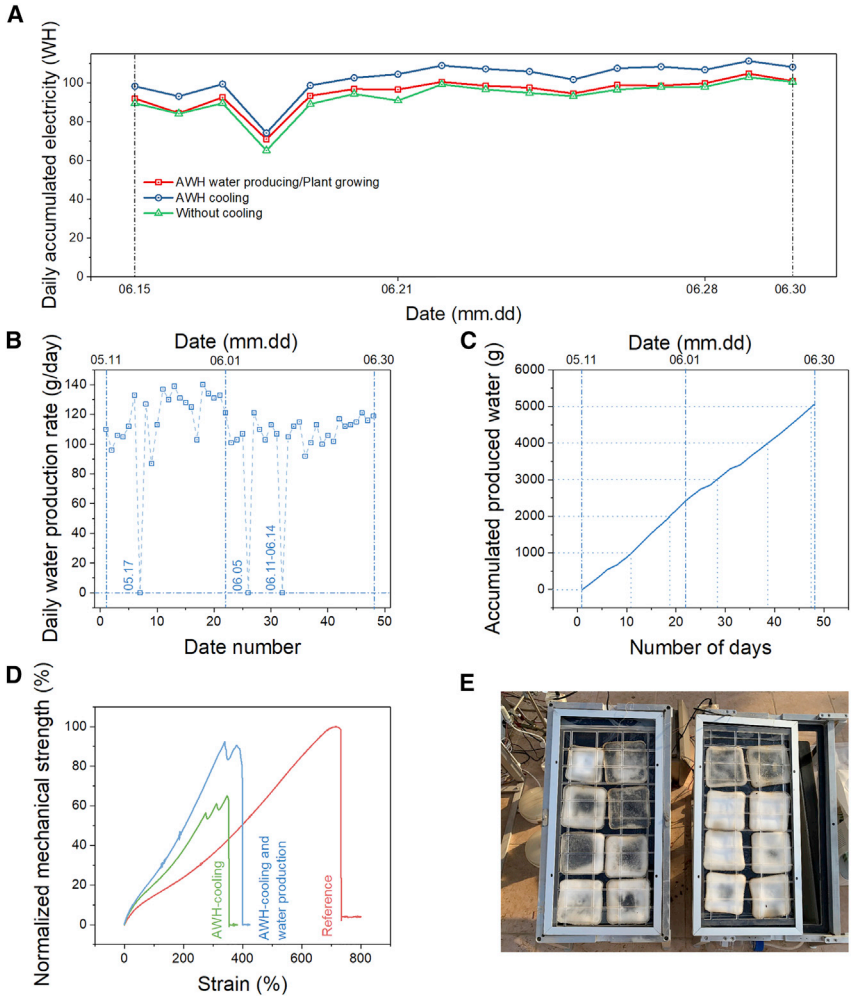

Figure 5. Evaluation of WEC^{2}P system performance

(A) Daily accumulated electricity generation records.

(B and C) Daily water production rate (B) and accumulated water production (C) during the entire AWH water-producing process.

(D) Mechanical stability curve of PAM-$CaCl_2$ hydrogel. The blue and the green profiles were acquired from the samples after the field test, while the red reference profile was obtained from the hydrogel prior to the field test.

(E) Digital photo of the backside of AWH-PV module after the 3-month field test. The dusty color of the hydrogel was due to the soiling by the ambient dusts during the test. Left: AWH-PV cooling and water-producing module is shown. Right: AWH-PV cooling module is shown.

16 when the foliage of the tallest plants reached the PGU ceiling when the average stem height was around 18 cm.

The electricity generation performance during the plant growing test was monitored. The power and temperature of PV panels were similar to the trend observed in the AWH cooling and fresh water producing test section. (Figure S20) The daily electricity generation rate was slightly decreased to ~100 Wh/day (Figure 5A). The accumulated electricity generation by "AWH-water and crop production mode," AWH cooling, and without cooling module was 1,519.2 Wh (527.5 Wh/m^2/day), 1,638.2 Wh (568.8 Wh/m^2/day), and 1,497.9 Wh (520.1 Wh/m^2/day), respectively. The electricity generation increment for "AWH-water production

Please cite this article in press as: Li et al., An integrated solar-driven system produces electricity with fresh water and crops in arid regions, Cell Reports Physical Science (2022), https://doi.org/10.1016/j.xcrp.2022.100781

mode" and AWH cooling was 1.4% and 9.4% compared with the PV panel without cooling.

The daily water production rate and the total collected water during the entire AWH water-producing process have been summarized in Figures 5B and 5C. The total collected water during the entire AWH water producing test, including both water production and crop production (from May 11 to June 30, 2021) was ~5.1 L, leading to an average AWH water production rate of ~0.6 L/m^2/day. The overall solar energy efficiency was calculated to be 23.1% during the AWH water-producing process. The mechanical stability of the PAM-$CaCl_2$ hydrogel was based on the strain-stress test (Figure 5D). The strain of the original PAM-$CaCl_2$ hydrogel was measured to 720%. After the 3-month test, the mechanical stability of the hydrogel was weakened, with the strain declining to 360% and 400% for AWH-PV cooling and AWH-PV cooling and water-producing batch, respectively. Figure 5E displays a digital photo of the AWH cooling layer, showing the PAM-$CaCl_2$ hydrogel still attached in place to the backside of the PV panel but with dust soiled on its surface.

DISCUSSION

During the operation of WEC^{2}P, one of the key factors is to maximize the mass transfer rate of water vapor for both the water vapor sorption and desorption process. With the cooling layer covering only the PV cell, the interval between the adjacent hydrogels provides additional airflow channels and extra water vapor sorption and evaporation surface, which can further increase the water vapor sorption and desorption kinetics during the operation. Considering the possible heat blockage by the anti-corrosion PE film, the thermal resistance is calculated based on the following equation:[39]

$$R_{PE} = \frac{\Delta x}{A_{PE} \times k}, \qquad \text{(Equation 1)}$$

where R_{PE}, Δx, and A_{PE} are the thermal resistance (K/W), thickness (4×10^{-5} m), and the cross-sectional area (~0.18 m^2) parallel to the PV panel (perpendicular to the path of heat flow) of PE film, respectively. k is the thermal conductivity of PE (0.5 W/m·K). Thus, the total thermal resistance of the PE film is calculated to be 4.4×10^{-4} K/W, which is considered negligible. Since the thermal conductivity of air (i.e., ~0.026 W/m·K) is much lower than that of PE, the close and even contact between the cooling layer and the PV panel is essential. The self-adhesive property of the PAM-$CaCl_2$ hydrogel and fixation frame ensure an effective heat transfer from the PV panel to the cooling layer in this work.

The electricity generation increment in this work was ~8%–10%, which is lower than our previous work (i.e., 13%–19%). In addition to the differences in the field test conditions, one major reason was the use of MPPT system and lead-acid battery as the load of PV panels during the daytime operation in this work, which allows the power flow out from the PV panel to be at its maximum output power (MOP). The MPPT system tracks the MOP of PV panels to ensure that the output power flowing to the load is always at its maximum. Meanwhile, the resistance of the lead-acid battery is dynamically changed during the charging process. Thereby, the charging power is adjusted accordingly by the MPPT system, which decreases with increasing battery levels. These two factors combined reduce the apparent significance of temperature differences and contribute to a lowered electricity generation increment in this work.

The working principle of the AWH system is based on the varying nature of the ambient conditions during the day-and-night cycle. When the humidity is high and

the temperature is low at night, water vapor sorption is facilitated. On the other hand, when the humidity is low and the temperature is high during the daytime, the evaporation process and thus cooling is promoted, leading to a higher evaporative cooling performance; for the AWH-water collection mode, water production is conducted in the sealed chamber, which does not require humidity input. In the water collection tests of this work, aerial humidity mainly influences the amount of water captured by water vapor sorbent during the night. Since the water vapor sorption component of the hydrogel is hygroscopic $CaCl_2$ salt, RH influences the sorption equilibrium of $CaCl_2$. Thus, the water sorption behavior is expected to be different and thereby the efficacy of AWH will be affected under different ambient aerial RH conditions.

Strong solar irradiation and lack of water resources in the arid and semi-arid regions are the two major challenges in agricultural development. Due to the high ambient temperature, low humidity, and abundant solar energy, the transpiration of leaf plants is usually strong to avoid overheating. The PGU deployed in the arid and semi-arid regions should minimize water usage and ensure sufficient heat removal. Our test has demonstrated that the temperature and humidity inside the PGU during the daytime can reach more than 70°C and RH ~100%. The overheated space can cause the death of the plant, and the saturated humidity can block the water transfer process and lead to plant diseases, such as fungi growing, rotting, etc.[40–43] Thereby, a sunlight-shielding net was used to cover the PGU and tune the penetrated solar irradiance by controlling the layers and thickness of the shielding net. With the sunlight partially shielded, the internal temperature of the PGU during the plant growing test remained only ~5°C higher than the ambient and did not exceed 50°C throughout the test. Besides, one of the sidewalls of the PGU was replaced with a perforated board to allow airflow and to maintain the RH level inside the PGU at 80%–90%, which provides sufficient humidity gradient for transpiration but with minimized water loss. The ratio of PV panel area to cropping area ($R_{PV/C}$) is an important factor that describes the irrigation capacity of WEC^{2}P. In our case, $R_{PV/C}$ was calculated to be 2:1, based on the water productivity and water consumption data obtained from the field test (Note S6). However, this ratio is highly variable, depending on several factors, such as the ambient conditions, location, seasons, and types of crops. Further studies should aim at achieving a smaller $R_{PV/C}$ value from both materials and engineering points of view.

The electricity generation increment of the AWH-PV module is closely related to the solar irradiance and ambient conditions. The peak solar irradiance and the average daily solar irradiance determine the peak heat generation rate and the upper limit of the daily electricity generation rate. The daytime temperature and humidity influence the temperature and humidity gradient between the surrounding ambient and PV panel and AWH cooling layer, while the nighttime humidity influences the water storing performance of the AWH cooling layer at night. The average wind speed (Note S5; Figures S10, S15, and S21) determines the effectiveness of convective heat transfer.

The electricity generation of the AWH-PV module is slightly different in the three field tests. April had the highest average daily solar irradiance (i.e., 5.37 kWh/m^2) and peak solar irradiance (850–1,000 W/m^2 in most cases) among all three testing months. The sufficient humidity during the night in April means water can be readily stored, and the low humidity during daytime facilitates the evaporation process, leading to the enhanced evaporative cooling power and thus most increased electricity generation among all.

Please cite this article in press as: Li et al., An integrated solar-driven system produces electricity with fresh water and crops in arid regions, Cell Reports Physical Science (2022), https://doi.org/10.1016/j.xcrp.2022.100781

The second test (i.e., AWH cooling and fresh water producing test) covered the mid- and late-May and early June, during which there was the lowest peak solar irradiance (i.e., ~700 W/m^2), an increased ambient temperature, and the highest average daytime humidity. The vapor pressure difference between the AWH cooling layer and the surrounding ambient was reduced during the daytime, which slowed down the evaporation process during operation and led to a reduced evaporative cooling power of the device. Furthermore, the reduced sunlight irradiance (i.e., 5.24 KWh/m^2) represented a lower heat generation rate from the PV panel. Considering the increased ambient temperature, heat dissipation could be suppressed due to the reduced temperature gradient between the PV-AWH module and the ambient. These factors resulted in an average electricity generation increment of 7.9%.

The ambient condition in the third field test (crop production feasibility test of WEC^{2}P in field conditions) was slightly changed. Even though the peak solar irradiance during the plant growing test was slightly higher than that of the other two tests (i.e., 750–800 W/m^2). The average daily sunlight irradiance, due to the frequently cloudy and dusty days in mid-June, was actually the lowest among all (5.13 kWh/m^2). Due to this reason, the daily electricity generation performance was the lowest on average among others. The ambient temperature, as well as the daytime humidity, was slightly lower, while the humidity during the night was high. This working condition improved the evaporation process by increasing the humidity gradient and enhanced the heat dissipation process due to the increased temperature gradient. The power generation increments were evaluated to be 1.4% and 9.4% for the AWH-water production mode and AWH-PV cooling mode, respectively. The high humidity inside the condensation chamber hinders the evaporation process, leading to a lowered evaporative cooling efficiency. In contrast, the cooling layer is exposed to the ambient in the AWH-PV cooling mode, where, in addition to a strong convective heat transfer, the surrounding ambient airflow also facilitates the evaporative cooling by effectively dissipating the evaporated water vapor to the ambient and thus helps maintain a relatively lower humidity around the cooling layer. Possible solutions to mitigate such a cooling efficiency decrease include the use of a heat fin on the outside of the condensation chamber to promote heat dissipation.

Due to the strong sunlight reflection from the ground and the high temperature of the PV panel, the aging of the polymer-based sorbent is inevitable. The degree of the material strength losses is correlated with the working temperature and the aging time.[44–46]

This work bridges the gap between material, engineering, and agronomy: experiences from the matured agronomy sectors can be used to guide the engineering design of the WEC^{2}P,[33] while the new materials and technologies will help to address the existing issues in the water-energy-food nexus.[24–27] The further development of WEC^{2}P certainly requires multidisciplinary inputs.

In summary, we have successfully developed a self-sustained, integrated water-electricity-crop co-production system (WEC^{2}P) that can produce extra electricity, fresh water, and crops in arid regions. The integrated system can locally generate clean water for irradiation purposes and does not require long-distance water transportation when deployed in arid regions. This strategy has the potential to make a solid contribution to the global water-energy-food nexus, generate electricity and produce water for remote and off-grid communities, improve food security in arid and semi-arid regions, and do so in a sustainable manner.

Please cite this article in press as: Li et al., An integrated solar-driven system produces electricity with fresh water and crops in arid regions, Cell Reports Physical Science (2022), https://doi.org/10.1016/j.xcrp.2022.100781

EXPERIMENTAL PROCEDURES

Resource availability

Lead contact

Further information and requests for the resources are available from the lead contact, Peng Wang (peng.wang@kaust.edu.sa).

Materials availability

This study did not generate unique materials.

Data and code availability

The data that support the findings of this study are available from the lead contact on reasonable request.

Materials

The PV panels with the panel dimension of 60 × 30 cm and the MPPT systems were purchased from Shanghai Sui-Ying. The rated open-circuit voltage (V_{OC}) of the PV panels is 18 V, and each PV panel consists of eight pieces of 12 × 12 cm PV cells. Acrylamide (AM) (99%) and potassium persulfate (KPS) (99%) were purchased from Acros Organics. N,N′-methylenebis(acrylamide) (MBAA) (99%), N,N,N′,N′-tetramethylethylenediamine (TEMED) (99%), and calcium chloride ($CaCl_2$) were purchased from Sigma-Aldrich. Deionized water (DI water) (18.2 MΩ) was generated from a Milli-Q system (Merck) and was used throughout the cooling layer synthesis process.

Synthesis of AWH cooling layer

The synthesis of PAM-$CaCl_2$ hydrogel cooling layer was in accord with our previous studies, however, with some slight modifications to fulfill the requirements on an enlarged scale. Briefly, 200 g of AM was dissolved in 1,000 mL of DI water followed by vigorous stirring for 10 min. The AM aqueous solution was then purged with nitrogen gas to eliminate the dissolved oxygen. Then, 0.1 g of MBAA and 1 g of KPS were added to the AM solution as cross-linking agent and initiator, respectively. After the as-formed mixture was stirred for 5 min under nitrogen atmosphere, 500 μL of TEMED was added under stirring as the cross-linking accelerator. Finally, the solution was transferred into 12 × 12 × 0.8 cm modes and was settled at room temperature in the nitrogen atmosphere overnight to get PAM hydrogel. The as-prepared PAM hydrogel was further freeze dried at −80°C (FreeZone 2.5 Plus, LABCONCO) and subsequently immersed in the 0.4 g/mL $CaCl_2$ solution for 1 week under ambient conditions to fabricate the PAM-$CaCl_2$ hydrogel.

Device assembly

The backside of the commercial PV panels was first coated with a layer of PE film (~0.04 mm in thickness) to prevent possible corrosion by the sorbents. The as-obtained PAM-$CaCl_2$ hydrogel was then directly attached to the backside of each individual PV cell in the PV panels via its self-adhesion properties. A poly (methyl methacrylate) (PMMA) plate-shaped frame was installed by spring bolts to reinforce the adhesion of PAM-$CaCl_2$ hydrogel with PV panel and secure their close contact. The as-assembled device was denoted as AWH-PV module.

Establishment of the field test

There were four PV panels used for the field test, including three panels for regular tests and one spare panel for backup. The PV panels were installed on the test frames and were tilted 22° to the ground and facing to the south. Environmental conditions, including ambient temperature, relative humidity, solar irradiance and wind speed, were real-time measured and recorded through a computer-controlled data

collection system. In order to make the test reflect the actual application scenario, the PV panels were connected with the MPPT system, and their power generation performance was monitored and recorded by coulomb meters. Each PV panel was considered as an independent module and was connected with an MPPT system and a 12-V lead-acid battery. Furthermore, each module was connected with a total of 20-W light-emitting diode (LED) light strips as a load to discharge the battery at night when the PV panel was not in operation. A series of thermal couples was used to measure the temperature of PV panels, and the temperature data were also recorded.

Pre-test PV panel calibration

In order to investigate the consistency of the four PV panels that were implemented for the field test, a 7-day pre-test was conducted from 7:00 a.m. March 19 to 7:00 p.m. March 25, 2021. All the four PV panels without any modifications (i.e., installation of cooling layer and condensation chamber) were investigated under the same field condition, and their averaged conversion efficiency during the 7-day test was calculated based on the following equations:

$$\eta_{PV} = \frac{E_{electricity}}{E_{solar}} \times 100\%; \quad \text{(Equation 2)}$$

$$E_{solar} = \int P_{solar} \cdot A \cdot dt; \quad \text{(Equation 3)}$$

$$E_{electricity} = \int P_{PV} \cdot dt, \quad \text{(Equation 4)}$$

where η_{PV} is the averaged conversion efficiency of the PV panel during the 7-day test, E_{solar} and $E_{electricity}$ are the accumulated solar irradiance and generated electricity during the test (Wh), P_{solar} and P_{PV} are the solar irradiance (W/m^2) and power of PV panel (W), A is the area of PV cell (m^2), and t is time (h).

AWH-PV cooling test and electricity generation evaluation

In the AWH-PV cooling test, two PV panels were installed with an AWH cooling layer (AWH cooling one and AWH cooling two) and another one remained unmodified (without cooling). The test was started at 7:00 a.m. on April 1, 2021 and finished at 7:00 p.m. May 10, 2021.

AWH cooling and fresh water producing test

In the AWH-PV cooling and fresh water production test, one PV panel was installed with an AWH cooling layer and aluminum alloy condensation chamber (denoted as ''AWH water producing''). The condensation chamber was opened at 7:00 p.m. for the atmospheric water absorption process and was closed at 7:00 a.m. the next day to proceed with the water condensation process. At the bottom of the condensation chamber, a cotton wick was used to transport the condensed water through the opened nozzle to the glass container outside the chamber (denoted as ''collection bottle''). The water productivity was recorded at 7:00 p.m. every day during the test. Two 2-L-capacity glass bottles were used as reservoir bottles to store the collected water from air for further use in the next phase of the test. The other two PV panels' configurations remained unchanged (AWH cooling and without cooling).

Crop production feasibility test of WEC^{2}P in field conditions

The WEC^{2}P field test was performed from June 15 to June 30, 2021. Briefly, a bench-scale PGU (dimension 500 × 270 × 340 mm) was assembled based on some

modifications of a commercialized PGU (Haier SPZW-A01WU1). The original electronic parts of the PGU were disabled and dismounted. Besides, one of its sidewalls was replaced with a perforated board and the entire device was covered with a commercialized and white-colored sunlight-shielding net to control the internal humidity and temperature. The planting soil was a mixture of sand (obtained from the desert near the campus) and potting soil (Sungro Metro-Mix 360) in a weight ratio of 1:1 to supply sufficient nutrients during the field test. Water spinach (*I. aquatica*) was used as the example plant for the WEC^{2}P field test. The PGU was opened and closed alternatively during the night from 7:00 p.m. to 7:00 a.m. the next day and 7:00 a.m. to 7:00 p.m. the same day. Since the prototype deployed in the field test is likely insufficient to produce enough water to supply the plants' daily irrigation demand in the current experiment, the stored water in the reservoir bottles from the previous phase of the test was involved to fill up the gap. The soil bath was replenished with ~150 mL of water every evening either solely from the collected water during the daytime or from the collected water during the daytime and from the preserved water from reservoir bottles combined. The stem height of the water spinach was recorded every morning from June 16 (the next morning after sowing) to July 1 (the next morning after the AWH-water producing test), and a picture of the plant was taken at the same time. In addition, a control experiment based on a 3D printed soil bath with a nine-hole stencil was conducted; all the test conditions and parameters remain the same, however, without the PGU and atmospheric water irrigation.

The overall solar energy efficiency during the AWH water-producing process was calculated based on the following equations.

$$\eta_{solar} = \frac{E_{electricity,WP} + E_{water}}{E_{solar,WP}} \times 100\%; \quad \text{(Equation 5)}$$

$$E_{solar,WP} = \int P_{solar,WP} \cdot A \cdot dt; \quad \text{(Equation 6)}$$

$$E_{electricity,WP} = \int P_{PV,WP} \cdot dt; \quad \text{(Equation 7)}$$

$$E_{water} = \frac{m_{water} \cdot \Delta H_{vap,water}}{3600\ J/WH}, \quad \text{(Equation 8)}$$

where η_{solar} is the overall solar energy efficiency; $E_{solar,WP}$, E_{water}, and $E_{electricity,WP}$ are the accumulated solar irradiance (Wh), energy consumed by water producing (Wh), and generated electricity during the water producing test (Wh); m_{water} is the accumulated water production during the test (kg); and $\Delta H_{vap,water}$ is the enthalpy of vaporization of water (2,266 kJ/kg).

Characterization

The concentration of metallic ions and the total organic components (TOCs) in the collected water was measured by an Agilent 5110 inductively coupled plasma-optical emission spectroscopy (ICP-OES) and a Shimadzu TOC-L TOC analyzer, respectively. The infrared image was taken by an FLIR A655 IR camera. The mechanical property of the hydrogel cooling layer was analyzed using a Universal Testing Machine (Instron 5944).

SUPPLEMENTAL INFORMATION

Supplemental information can be found online at https://doi.org/10.1016/j.xcrp.2022.100781.

ACKNOWLEDGMENTS

The authors are grateful to the KAUST for very generous financial support.

AUTHOR CONTRIBUTIONS

R.L. and P.W. designed the experiments. R.L. conducted the experiments. R.L. and M.W. analyzed the data. R.L. and P.W. wrote the paper. All the authors commented on the manuscript drafts.

DECLARATION OF INTERESTS

The authors declare no competing interests.

Received: November 21, 2021
Revised: January 5, 2022
Accepted: January 28, 2022
Published: March 1, 2022

REFERENCES

1. The Food and Agriculture Organization (FAO) of the United Nations (2014). The Water-Energy-Food Nexus. A new approach in support of food security and sustainable agriculture. https://www.fao.org/policy-support/tools-and-publications/resources-details/en/c/421718/.
2. Endo, A., Tsurita, I., Burnett, K., and Orencio, P.M. (2017). A review of the current state of research on the water, energy, and food nexus. J. Hydrol. Reg. Stud. *11*, 20–30.
3. Al-Saidi, M., and Elagib, N.A. (2017). Towards understanding the integrative approach of the water, energy and food nexus. Sci. Total Environ. *574*, 1131–1139.
4. Sachs, J.D., Schmidt-Traub, G., Mazzucato, M., Messner, D., Nakicenovic, N., and Rockström, J. (2019). Six transformations to achieve the sustainable development goals. Nat. Sustain. *2*, 805–814.
5. Fuso Nerini, F., Sovacool, B., Hughes, N., Cozzi, L., Cosgrave, E., Howells, M., Tavoni, M., Tomei, J., Zerriffi, H., and Milligan, B. (2019). Connecting climate action with other sustainable development Goals. Nat. Sustain. *2*, 674–680.
6. The United Nations World Water Development Report 2020, Water and Climate Change, UNESCO. https://en.unesco.org/themes/water-security/wwap/wwdr/2020.
7. Perera, A.T.D., Nik, V.M., Chen, D., Scartezzini, J.-L., and Hong, T. (2020). Quantifying the impacts of climate change and extreme climate events on energy systems. Nat. Energy. *5*, 150–159.
8. Schmidhuber, J., and Tubiello, F.N. (2007). Global food security under climate change. Proc. Natl. Acad. Sci. U.S.A. *104*, 19703–19708.
9. Feron, S., Cordero, R.R., Damiani, A., and Jackson, R.B. (2021). Climate change extremes and photovoltaic power output. Nat. Sustain. *4*, 270–276.
10. World Health Organization (WHO) and the United Nations Children's Fund (UNICEF) Joint Monitoring Programm (JMP) (2021). Progress on Household Drinking Water, Sanitation and Hygiene: 2021 Update. https://www.who.int/publications/i/item/9789240030848.
11. Bain, R., Johnston, R., Mitis, F., Chatterley, C., and Slaymaker, T. (2018). Establishing sustainable development goal baselines for household drinking water, sanitation and hygiene services. Water *10*, 1711–1729.
12. International Energy Agency (IEA) (2020). World energy outlook 2020. https://www.iea.org/reports/world-energy-outlook-2020.
13. The Food and Agriculture Organization (FAO) of the United Nations (2020). The state of food security and nutrition in the world, Rome. https://www.fao.org/3/ca9692en/online/ca9692en.html#chapter-executive_summary.
14. International Renewable Energy Agency (IRENA) (2015). Renewable energy capacity statistics 2015. https://www.irena.org/publications/2015/Jun/Renewable-Energy-Capacity-Statistics-2015.
15. Dolan, F., Lamontagne, J., Link, R., Hejazi, M., Reed, P., and Edmonds, J. (2021). Evaluating the economic impact of water scarcity in a changing world. Nat. Commun. *12*, 1915.
16. Zhou, Y., and Tol, R.S.J. (2005). Evaluating the costs of desalination and water transport. Water Resour. Res. *4*, W03003.
17. Lin, B., and Wu, W. (2017). Cost of long distance electricity transmission in China. Energy Policy *109*, 132–140.
18. Wang, W., Aleid, S., and Wang, P. (2020). Decentralized Co-generation of fresh water and electricity at point of consumption. Adv. Sustain. Syst. *4*, 2000005.
19. Chen, Q., Burhan, M., Akhtar, F.H., Ybyraiymkul, D., Shahzad, M.W., Li, Y., and Ng, K.C. (2021). A decentralized water/electricity cogeneration system integrating concentrated photovoltaic/thermal collectors and vacuum multi-effect membrane distillation. Energy *230*, 120852.
20. Zhou, X., Zhang, P., Zhao, F., and Yu, G. (2020). Super moisture absorbent gels for sustainable agriculture via atmospheric water irrigation. ACS Mater. Lett. *2*, 1419–1422.
21. Shan, H., Pan, Q., Xiang, C., Poredos, P., Ma, Q., Ye, Z., Hou, G., and Wang, R. (2021). High-yield solar-driven atmospheric water harvesting with ultra-high salt content composite encapsulated in porous membrane. Cell Rep. Phys. Sci. *2*, 100664.
22. Tu, Y., Wang, R., Zhang, Y., and Wang, J. (2018). Progress and expectation of atmospheric water harvesting. Joule *2*, 1452–1475.
23. Lord, J., Thomas, A., Treat, N., Forkin, M., Bain, R., Dulac, P., Behroozi, C.H., Mamutov, T., Fongheiser, J., Kobilansky, N., et al. (2021). Global potential for harvesting drinking water from air using solar energy. Nature *598*, 611–617.
24. Yang, L., Nandakumar, D.K., Miao, L., Suresh, L., Zhang, D., Xiong, T., Vaghasiya, J.V., Kwon, K.C., and Tan, S.C. (2020). Energy harvesting from atmospheric humidity by a hydrogel-integrated ferroelectric-semiconductor system. Joule *4*, 176–188.
25. Zhang, Y., Nandakumar, D.K., and Tan, S.C. (2020). Digestion of ambient humidity for energy generation. Joule *4*, 2532–2536.
26. Yang, J., Zhang, X., Qu, H., Yu, Z.G., Zhang, Y., Eey, T.J., Zhang, Y., and Tan, S.C. (2020). A moisture-hungry copper complex harvesting air moisture for potable water and autonomous urban agriculture. Adv. Mater. *32*, 2002936.
27. Zhang, X., Yang, J., Qu, H., Yu, Z.G., Nandakumar, D.K., Zhang, Y., and Tan, S.C. (2021). Machine-learning-assisted autonomous humidity management system based on solar-regenerated super hygroscopic complex. Adv. Sci. *8*, 2003939.
28. Ziar, H., Manganiello, P., Isabella, O., and Zeman, M. (2021). Photovoltatronics: intelligent PV-based devices for energy and information applications. Energy Environ. Sci. *14*, 106–126.

29. Parida, B., Iniyan, S., and Goic, R. (2011). A review of solar photovoltaic technologies. Renew. Sust. Energ. Rev. *15*, 1625–1636.

30. Jean, J., Brown, P.R., Jaffe, R.L., Buonassisi, T., and Bulović, V. (2015). Pathways for solar photovoltaics. Energy Environ. Sci. *8*, 1200–1219.

31. Wang, W., Aleid, S., Shi, Y., Zhang, C., Li, R., Wu, M., Zhuo, S., and Wang, P. (2021). Integrated solar-driven PV cooling and seawater desalination with zero liquid discharge. Joule *5*, 1873–1887.

32. Al-Ibrahim, A., Al-Abbadi, N., and Al-Helal, I. (2006). PV greenhouse system-system description, performance and lesson learned. Aceta Hortic. *710*, 251–264.

33. Li, R., Shi, Y., Wu, M., Hong, S., and Wang, P. (2020). Photovoltaic panel cooling by atmospheric water sorption–evaporation cycle. Nat. Sustain. *3*, 636–643.

34. Liu, L., Wang, Q., Lin, H., Li, H., Sun, Q., and wennersten, R. (2017). Power generation efficiency and prospects of floating photovoltaic systems. Energy Proced. *105*, 1136–1142.

35. Khan, J., and Arsalan, M.H. (2016). Solar power technologies for sustainable electricity generation – a review. Renew. Sust. Energ. Rev. *55*, 414–425.

36. Li, R., Wu, M., Shi, Y., Aleid, S., Wang, W., Zhang, C., and Wang, P. (2021). Hybrid water vapor sorbent design with pollution shielding properties: extracting clean water from polluted bulk water sources. J. Mater. Chem. A. *9*, 14731–14740.

37. Li, R., Shi, Y., Alsaedi, M., Wu, M., Shi, L., and Wang, P. (2018). Hybrid hydrogel with high water vapor harvesting capacity for deployable solar-driven atmospheric water generator. Environ. Sci. Technol. *52*, 11367–11377.

38. World Health Organization (WHO). (2017). Guidelines for Drinking-Water Quality, 4th edition, incorporating the 1st addendum. https://www.who.int/publications/i/item/9789241549950.

39. Bergman, T.L., Incropera, F.P., DeWitt, D.P., and Lavine, A.S. (2011). Fundamentals of Heat and Mass Transfer (John Wiley & Sons).

40. Velásquez, A.C., Castroverde, C.D.M., and He, S.Y. (2018). Plant–pathogen warfare under changing climate conditions. Curr. Biol. *28*, R619–R634.

41. Aung, K., Jiang, Y., and He, S.Y. (2018). The role of water in plant–microbe interactions. Plant J. *93*, 771–780.

42. Jagadish, S., Craufurd, P., and Wheeler, T. (2007). High temperature stress and spikelet fertility in rice (Oryza sativa L.). J. Exp. Bot. *58*, 1627–1635.

43. Li, B., Gao, K., Ren, H., and Tang, W. (2018). Molecular mechanisms governing plant responses to high temperatures. J. Integr. Plant Biol. *60*, 757–779.

44. Xiong, B., Loss, R.D., Shields, D., Pawlik, T., Hochreiter, R., Zydney, A.L., and Kumar, M. (2018). Polyacrylamide degradation and its implications in environmental systems. Npj Clean. Water *1*, 17.

45. Xiong, C., Wei, F., Li, W., Liu, P., Wu, Y., Dai, M., and Chen, J. (2018). Mechanism of polyacrylamide hydrogel instability on high-temperature conditions. ACS Omega *3*, 10716–10724.

46. Caulfield, M.J., Hao, X., Qiao, G.G., and Solomon, D.H. (2003). Degradation on polyacrylamides. Part II. Polyacrylamide gels. Polymer *44*, 3817–3826.